Zhang et al. Nanoscale Research Letters (2017) 12:43
DOI 10.1186/s11671-016-1811-0

Nanoscale Research Letters

NANO EXPRESS Open Access

Enhancement of Perovskite Solar Cells Efficiency using N-Doped TiO_2 Nanorod Arrays as Electron Transfer Layer

Zhen-Long Zhang[1], Jun-Feng Li[1], Xiao-Li Wang[1], Jian-Qiang Qin[1], Wen-Jia Shi[1], Yue-Feng Liu[1], Hui-Ping Gao[1] and Yan-Li Mao[1,2*]

Abstract

In this paper, N-doped TiO_2 (N-TiO_2) nanorod arrays were synthesized with hydrothermal method, and perovskite solar cells were fabricated using them as electron transfer layer. The solar cell performance was optimized by changing the N doping contents. The power conversion efficiency of solar cells based on N-TiO_2 with the N doping content of 1% (N/Ti, atomic ratio) has been achieved 11.1%, which was 14.7% higher than that of solar cells based on un-doped TiO_2. To get an insight into the improvement, some investigations were performed. The structure was examined with X-ray powder diffraction (XRD), and morphology was examined by scanning electron microscopy (SEM). Energy dispersive spectrometer (EDS) and Tauc plot spectra indicated the incorporation of N in TiO_2 nanorods. Absorption spectra showed higher absorption of visible light for N-TiO_2 than un-doped TiO_2. The N doping reduced the energy band gap from 3.03 to 2.74 eV. The photoluminescence (PL) and time-resolved photoluminescence (TRPL) spectra displayed the faster electron transfer from perovskite layer to N-TiO_2 than to un-doped TiO_2. Electrochemical impedance spectroscopy (EIS) showed the smaller resistance of device based on N-TiO_2 than that on un-doped TiO_2.

Keywords: Enhancement of efficiency, N-doped TiO_2 nanorod arrays, Electron transfer layer

Background

In recent years, extensive studies are focused on perovskite solar cells (PSCs) due to their outstanding properties, such as large absorption coefficient, electron-hole diffusion length, and high charge carrier mobility [1–5]. The power conversion efficiency (PCE) of perovskite solar cells has been over 22% [6]. Conventionally, perovskite solar cells consist of a perovskite layer sandwiched between an electron transfer material (ETM) layer and a hole transfer material (HTM) layer. Mesoporous TiO_2 has been used as the ETM in most of the perovskite solar cells [7, 8]. Compared with the mesoporous structure, one dimensional (1D) nanostructure has some advantages, such as easy pore filling of active layer or HTM, better electron transfer, and lower charge recombination [9, 10]. Therefore, TiO_2 nanorods (NRs) have been widely applied to perovskite solar cells [11, 12]. However, there are a mass of oxygen vacancies defects exist in pristine TiO_2 nanorods, which reduces the efficiency and stability of the perovskite solar cell [13].

In order to solve the issues, some methods have been adopted, such as metal doping [14, 15] and nonmetal doping [16]. It has been reported that N-doped TiO_2 as a photoanode of dye-sensitized solar cells (DSSCs) can improve the energy conversion efficiency due to the change of properties of TiO_2, such as electron lifetime prolongation, charge transfer resistance reduction, and visible light absorption extension [17, 18].

We wondered about the effect of N-doped TiO_2 on the performance of perovskite solar cells. Hence, in the present study, we synthesized N-doped TiO_2 (N-TiO_2) nanorod arrays with hydrothermal method and fabricated perovskite solar cells using them as electron transfer layer. The solar cell performance was optimized by changing the N doping contents. The PCE of solar cells based on N-TiO_2 with the N

* Correspondence: ylmao1@163.com
[1]School of Physics and Electronics, Henan University, Kaifeng 475004, China
[2]Institute for Computational Materials Science, Henan University, Kaifeng 475004, China

doping content of 1% (N/Ti, atomic ratio) has been achieved 11.1%, which was 14.7% higher than that of solar cells based on un-doped TiO_2. The possible mechanisms of enhancement were discussed based on some investigations.

Methods

Growth of TiO_2 Nanorod Arrays

Patterned fluorine-doped tin oxide (FTO)-coated glass substrate was cleaned by sonication for 20 min in detergent, acetone, 2-propanol, and ethanol, respectively. A TiO_2 compact layer was deposited by dipping the substrate in a 0.2 M $TiCl_4$ aqueous solution at 70 °C for 30 min. TiO_2 NRs were grown on the treated FTO substrate by a hydrothermal method in our previous report [19]. A 0.7 mL of titanium(IV) n-butoxide was added to a mixture of hydrochloric acid and deionized water. Subsequently, the pre-calculated amount of $CO(NH_2)_2$ was added to the solution (the nominal N/Ti atomic ratio, 0.5, 1, 2, and 3%) and stirred until it was completely dissolved. The FTO substrate was put into the solution and sealed in an autoclave. The autoclave was heated to 170 °C for several hours. The obtained TiO_2 nanorods film was rinsed and annealed at 500 °C for 60 min.

Materials Preparation

Methylammonium iodide (CH_3NH_3I) was synthesized with a reported method [20]. The precursor solution for perovskite film formation was obtained by mixing $PbCl_2$ and CH_3NH_3I in anhydrous *N*,*N*-dimethylformamide (DMF) at a 1:3 molar ratio at 60 °C overnight.

Solar Cell Fabrication

The perovskite film was formed by spin coating at 2000 rpm for 60 s in a glove box, and drying on a hotplate at 110 °C for 60 min. The HTM layer was obtained by spin coating a spiro-OMeTAD solution at 2000 rpm for 60 s. Finally, a gold layer was deposited on the top of the device by thermal evaporation.

Characterization

X-ray diffraction (XRD) patterns were measured using a diffractometer (DX-2700). Photocurrent–voltage (*I*–*V*) curves were carried out with a Keithley 2440 Source meter under AM 1.5 G illumination from a Newport Oriel Solar Simulator with an intensity of 100 mW/cm^2. A shadow mask was used to determine the active area of 0.1 cm^2. Morphologies and microstructures were performed using a scanning electron microscope (SEM, JEM-7001F, JEOL) equipped with an energy dispersive spectrometer (EDS). Absorption spectra were obtained with a UV–Vis spectrophotometer (Varian Cary 5000). Steady-state photoluminescence (PL) and time-resolved photoluminescence (TRPL) spectra were collected with a fluorometer (FLS 980E, Edinburgh Photonics). An electrochemical workstation (CHI660e, Shanghai CHI Co., Ltd.) was used to collect the electrochemical impedance spectroscopy (EIS) with a bias of 0.6 V.

Results and Discussion

TiO_2 nanorod arrays with different N doping contents were prepared, and perovskite solar cells based on them were fabricated. The *I*–*V* measurements were performed by reverse scan (RS) and forward scan (FS). The photovoltaic parameters were obtained by the average of reverse scan and forward scan for each device. The I_{sc}, V_{oc}, FF, and PCE of the solar cells in the study were obtained by an average of the data from 20 pieces of devices. Figure 1a shows the power conversion efficiency of solar cells dependence on nominal N doping contents. The PCE changes with the increase of N doping content, which reaches the maximum at the doping content of 1% (N/Ti, atomic ratio). Table 1 shows the photovoltaic parameters of the solar cells based on un-doped and 1% N-TiO_2 NRs. The I_{sc}, V_{oc}, FF, and PCE of the solar cells

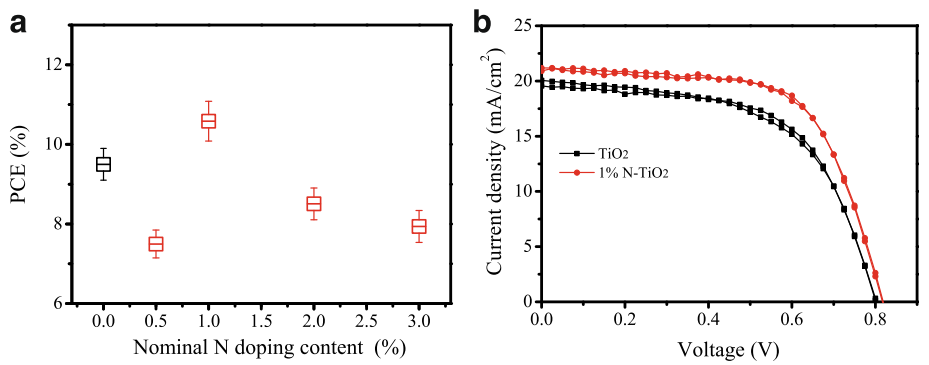

Fig. 1 **a** PCE of solar cells dependence on nominal N doping contents. The data were obtained from 20 pieces of devices for each of conditions. **b** *I*–*V* curves of best performance solar cells based on un-doped TiO_2 and 1% N-TiO_2 NRs

Table 1 Photovoltaic parameters of best performance solar cells based on the TiO_2 and N-TiO_2 NRs

Sample	V_{oc} (V)	I_{sc} (mA/cm^2)	FF	PCE (%)
TiO_2	0.80 ± 0.02	19.2 ± 0.0.6	0.62 ± 0.03	9.5 ± 0.3
1% N-TiO_2	0.82 ± 0.01	20.5 ± 0.7	0.65 ± 0.02	10.9 ± 0.2

based on N-TiO_2 NRs are enhanced compared with those based on un-doped TiO_2 NRs. The PCE of solar cells based on N-TiO_2 NRs is 14.7% higher than that of solar cells based on un-doped TiO_2 NRs. Figure 1b shows the *I*–*V* curves of best performance solar cells based on un-doped TiO_2 and 1% N-TiO_2 NRs.

Figure 2 shows the IPCE of the perovskite solar cells based on un-doped TiO_2 NRs and 1% N-TiO_2 NRs. The IPCE at the entire wavelength range of the cells based on N-TiO_2 NRs are larger than those on the un-doped TiO_2 NRs, which agree with the *I*–*V* measurements.

To get an insight into the enhancement, some investigations were performed. Figure 3 shows the XRD patterns of un-doped TiO_2 and 1% N-TiO_2 NRs. The peaks labeled with stars were assigned to SnO_2 (JCPDS card, 41-1445) on FTO substrate. The peak at 36.1° was assigned to the (101) planes of rutile TiO_2 (JCPDS card, 21-1276) [21]. For the XRD patterns of N-TiO_2 NRs, the peaks on N element were not observed. This could be due to the homogeneous distribution of N with Ti in the samples [22] and small amount of doping contents.

Figure 4 shows the XPS spectra of 1% N-TiO_2 NRs. Figure 4a shows the survey XPS spectrum. The peaks at 458.8 and 464.8 eV in Fig. 4b are attributed to the binding energy of Ti $2p_{3/2}$ and Ti $2p_{1/2}$, respectively. The peak located at 400.1 eV in Fig. 4c is attributed to N 1s [23]. The peak at 530.1 eV in Fig. 4d could be from O 1s. The XPS spectra demonstrated the successful doping of N in the

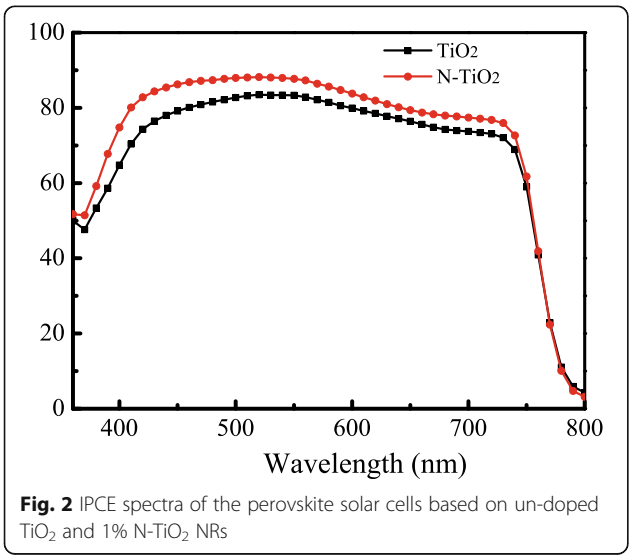

Fig. 2 IPCE spectra of the perovskite solar cells based on un-doped TiO_2 and 1% N-TiO_2 NRs

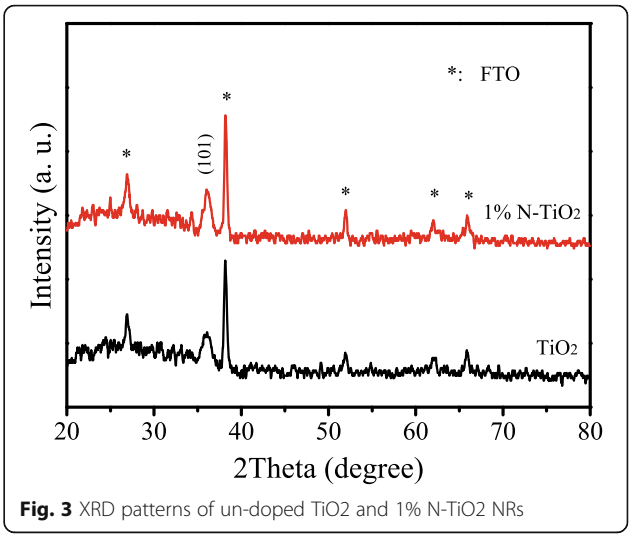

Fig. 3 XRD patterns of un-doped TiO2 and 1% N-TiO2 NRs

TiO_2 film, which was further confirmed by the EDS spectrum as shown in Additional file 1: Figure S1 (Supplementary Material).

Figure 5a, c shows the plane-view and cross-sectional SEM images of un-doped TiO_2 NRs, and Fig. 5b, d shows the plane-view and cross-sectional SEM images of 1% N-TiO_2 NRs. The diameter and length of the un-doped TiO_2 NRs were determined to be 48 ± 5 nm and 490 ± 15 nm, respectively. The diameter and length of the 1% N-TiO_2 NRs were determined to be 42 ± 6 nm and 480 ± 25 nm, respectively. The diameter of N-TiO_2 NRs is slightly decreased compared with that of un-doped TiO_2 NRs. The length distribution of N-TiO_2 NRs is more ununiform than that of un-doped TiO_2 NRs. From a view of large area (Additional file 1: Figure S2, Supplementary Material), there are some bluges on the sample surfaces due to the inhomogenous oritiation. There are more bluges on the surfaces of N-TiO_2 NRs compared with those of un-doped TiO_2 NRs. This could be attributed to the effect of N doping. Additional file 1: Figure S3 (Supplementary Material) shows the cross-sectional SEM images of the whole solar cells based on TiO_2 NRs. The bottom is the FTO glass. Pores of nanorods are filled by $MAPbI_{3-x}Cl_x$, on which a capping layer of perovskite was formed. The Spiro-OMeTAD layer is separated by the capping layer from nanorod films. The top layer is a thin Au film.

Figure 6a shows the UV–Vis absorption spectra of un-doped TiO_2 and 1% N-TiO_2 NRs. The absorption intensity of N-TiO_2 is stronger than that of un-doped TiO_2. The energy band gap (Eg) can be calculated based on the absorption spectra using the Tauc equation [24]. The Tauc curve is shown in Fig. 6b, in which Eg can be estimated to be 3.03 and 2.74 eV for un-doped TiO_2 and N-TiO_2 NRs, respectively. Compared with that of un-doped TiO_2, the energy band gap of N-TiO_2 becomes smaller.

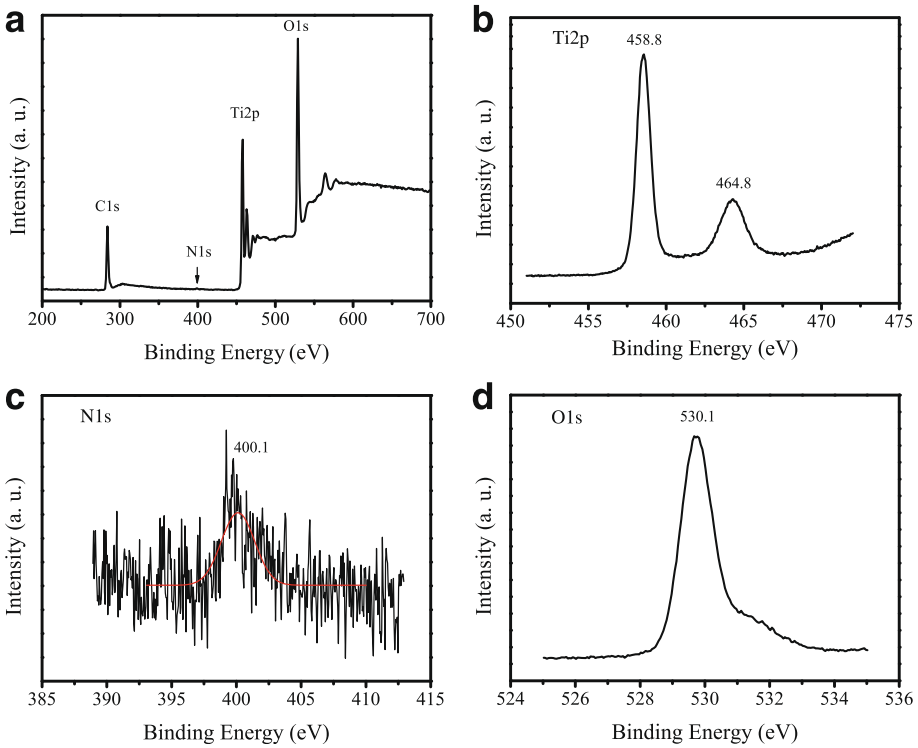

Fig. 4 XPS spectra of 1% N-TiO_2 NRs. **a** Survey XPS, **b** Ti 2p, **c** N 1s, and **d** O 1s

This could be attributed to the substitution location of N in the TiO_2 lattice, in which an O (Ti) atom is replaced by an N atom [25]. The conduction band offset between N-TiO_2 and $MAPbI_{3-x}Cl_x$ is larger than that between un-doped TiO_2 and $MAPbI_{3-x}Cl_x$ due to its narrow energy band gap, which might be one of the reasons to present a higher voltage for N-TiO_2-based solar cells [26].

PL is a suitable tool to study the efficiency of charge carrier trapping, migration, and transfer [27, 28]. Figure 7a shows the PL spectra of un-doped TiO_2/

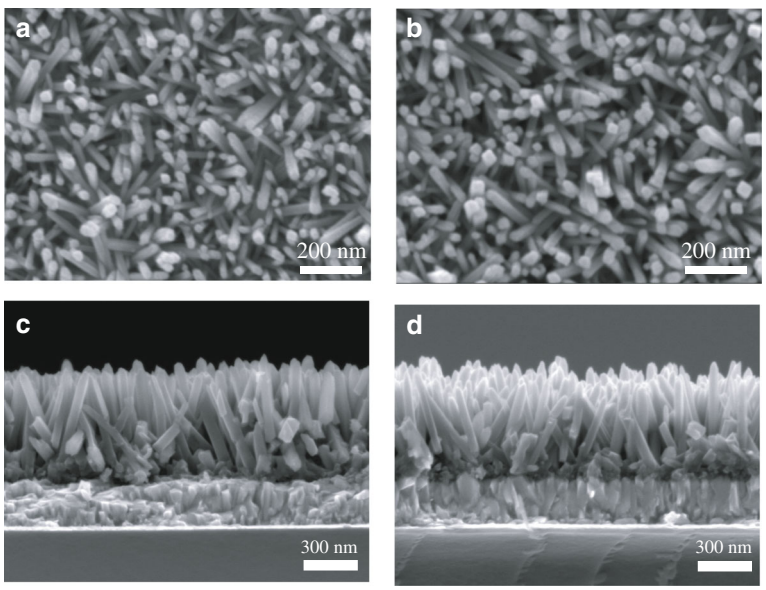

Fig. 5 Plane-view SEM images of un-doped TiO_2 (**a**) and 1% N-TiO_2 NRs (**b**). Cross-sectional SEM images of un-doped TiO_2 (**c**) and 1% N-TiO_2 NRs (**d**)

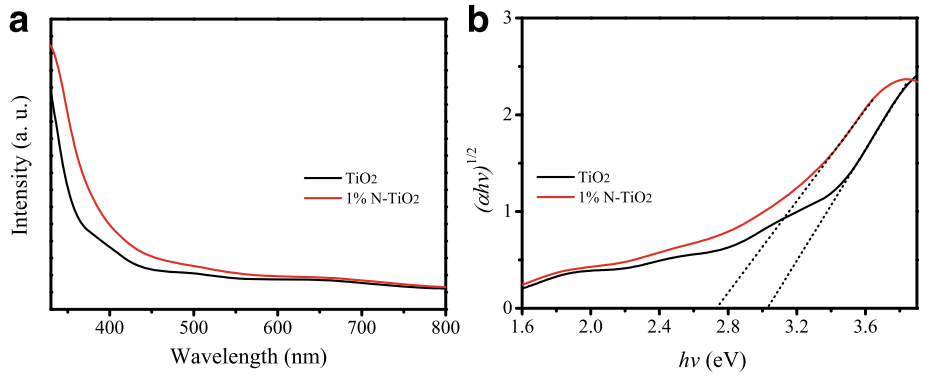

Fig. 6 a UV–Vis absorption spectra of un-doped TiO_2 and 1% N-TiO_2 NRs. **b** Tauc curves

$MAPbI_{3-x}Cl_x$ and 1% N-TiO_2/$MAPbI_{3-x}Cl_x$. The intensity of PL spectrum was decreased due to the electron transfer when the $MAPbI_{3-x}Cl_x$ film contacts with TiO_2 nanorod layer. The intensity decrease for N-TiO_2 is more significant than that for un-doped TiO_2, which indicates the electron transfer from $MAPbI_{3-x}Cl_x$ layer to N-TiO_2 is more effective than to un-doped TiO_2.

Figure 7b shows the TRPL spectra of un-doped TiO_2/$MAPbI_{3-x}Cl_x$ and 1% N-TiO_2/$MAPbI_{3-x}Cl_x$. The TRPL curves were analyzed with a bi-exponential decay function containing a fast decay (τ_1) component and a slow decay component (τ_2), and the detailed parameters are listed in Table 2. The fast decay component would be the result of free carrier transportation from $MAPbI_{3-x}Cl_x$ to TiO_2, and the slow decay component could be the result of radiative decay [29, 30]. In the case of un-doped TiO_2/$MAPbI_{3-x}Cl_x$, the fast decay time is 55.1 ns, and the slow decay time is 121.4 ns, while their weight fractions are 31.3 and 67.7%, respectively. Compared with those of un-doped TiO_2/$MAPbI_{3-x}Cl_x$, the fast decay lifetime of N-TiO_2/$MAPbI_{3-x}Cl_x$ is decreased to 36.4 from 55.1 ns, and the slow decay life time to 109.5 from 121.4 ns, while the weight fraction of fast decay is increased to 35.1 from 31.3%. This suggests that N-TiO_2/$MAPbI_{3-x}Cl_x$ interface presents a faster charge transfer and induced charge recombination than the un-doped TiO_2/$MAPbI_{3-x}Cl_x$ interface. The performance difference between the solar cells based on un-doped TiO_2 and N-doped TiO_2 NRs could be due to the property change of ETM, which affects the charge behavior in the interfaces [31, 32].

To understand the charge transfer behavior of the solar cells, electrochemical impedance spectrum (EIS) was measured. Figure 8a shows the Nyquist plots of solar cells that based on un-doped TiO_2 and 1% N-TiO_2 NRs. The EIS contains two RC arcs. The arc at high frequency is originated from the contact resistance of the interfaces and that at low frequency is attributed to recombination resistance (R_{rec}) and chemical capacitance (C_μ) of the device [33, 34]. Figure 8b shows an equivalent circuit which was applied to fit the EIS. Table 3 lists the fitting parameters. The solar cells based on N-TiO_2 present smaller series resistance and larger recombination resistance than those on un-doped TiO_2. This demonstrates that the charge transport ability was enhanced and the carrier recombination rate was induced for the device on N-TiO_2. There are many surface and

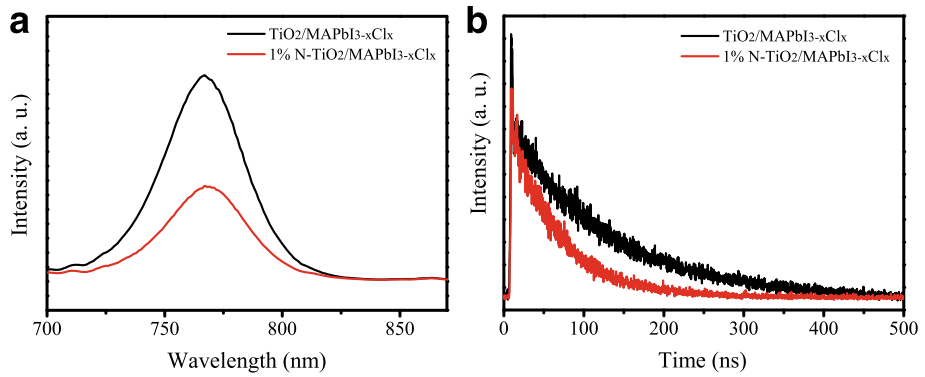

Fig. 7 a PL and **b** TRPL spectra of un-doped TiO_2/$MAPbI_{3-x}Cl_x$ and 1% N-TiO_2/$MAPbI_{3-x}Cl_x$

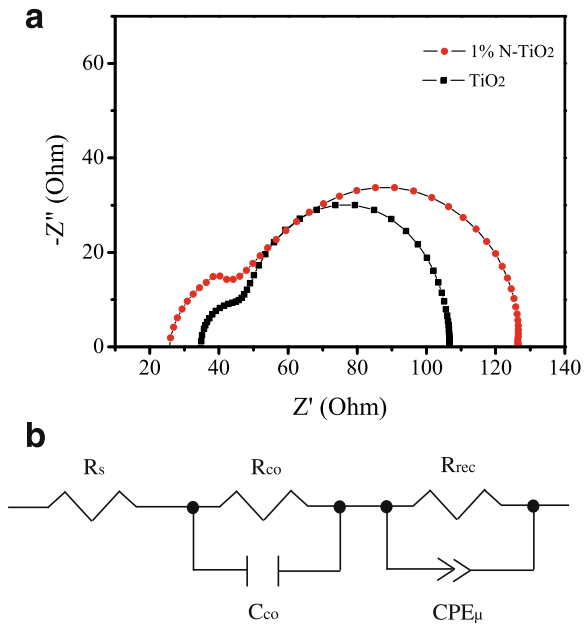

Fig. 8 a EIS spectra of solar cells that based on un-doped TiO_2 and 1% N-TiO_2 NRs based solar cells. **b** Equivalent circuit for fitting the EIS data

bulk trap states due to oxygen vacancies for TiO_2. It demonstrated that the incorporation of N atom into the lattice of TiO_2 can decrease the traps density probably due to oxygen vacancy reduction [18, 35]. The smaller series resistance of N-TiO_2 NRs could be due to the decreased traps density. The larger recombination resistance of N-TiO_2 NRs may be contributed to the inactive N element leading to the increase of surface resistance [36, 37].

Conclusions

In the present study, N-TiO_2 NRs were synthesized with hydrothermal method, and perovskite solar cells based on them were fabricated. Compared with the solar cells based on un-doped TiO_2, solar cells based on N-TiO_2 present an enhanced performance. The solar cell performance was optimized by changing the N doping contents. The PCE of solar cells based on N-TiO_2 with the N doping content of 1% (N/Ti, atomic ratio) has been achieved 11.1%, which was 14.7% higher than that of un-doped TiO_2-based solar cells. To explain this phenomenon, some investigations were performed. The results indicate that the larger V_{oc} could be due to the larger conduction band offset resulting from the smaller energy band gap for N-TiO_2, and the enlarged I_{sc} could be attributed to the faster electron transfer and reduced recombination rate for N-TiO_2 NRs. These induce the enhanced performance of the solar cells based on N-TiO_2 NRs.

Table 2 Parameters of the TRPL spectra

Sample	τ_1/ns	% of τ_1	τ_2/ns	% of τ_2
TiO_2 /$MAPbI_{3-x}Cl_x$	55.1	31.3	121.4	67.7
1% N-TiO_2 /$MAPbI_{3-x}Cl_x$	36.4	35.1	109.5	64.9

Table 3 Fitting parameters of EIS date

Sample	R_s/Ω	R_{co}/Ω	R_{rec}/Ω	CPE-T/F
TiO_2	34.8	59.3	12.7	6.3×10^{-6}
1% N-TiO_2	27.5	23.7	75.1	5.9×10^{-6}

Additional file

Additional file 1: Supplementary Material. **Figure S1.** EDS spectrum of 1% N-TiO_2 NRs. **Figure S2.** Plane-view SEM images of un-doped TiO_2 (A), and 1% N-TiO_2 NRs(B). **Figure S3.** Cross-sectional SEM image of perovskite solar cells. (DOCX 826 kb)

Acknowledgements
This work is supported by the Science and Technology Development Project of Henan Province (No.142102210389), National Science Research Project of Education Department of Henan Province (No.17A140005), and Program for Innovative Research Team (in Science and Technology) in University of Henan Province (No. 13IRTSTHN017), and NSFC-Henan Province Joint Fund (U1604144).

Authors' Contributions
Z-LZ, J-FL, and Y-LM carried out the main part of experiment and drafted the manuscript. The other authors provided assistance with the experimental measurements, data analysis, and the manuscript writing. All authors read and approved the final manuscript.

Competing Interests
The authors declare that they have no competing interests.

Received: 30 September 2016 Accepted: 26 December 2016
Published online: 17 January 2017

References
1. Stranks SD, Eperon GE, Grancini G, Menelaou C, Alcocer MJP, Leijtens T, Laura M, Herz M, Petrozza A, Snaith HJ (2013) Electron-hole diffusion lengths exceeding 1 micrometer in an organometal trihalide perovskite absorber. Science 342:341–344
2. Xing G, Mathews N, Sun S, Lim SS, Lam YM, Graetzel M, Mhaisalkar S, Sum TC (2013) Long-range balanced electronand hole-transport lengths in organicinorganic $CH_3NH_3PbI_3$. Science 342:344–347
3. Mei AY, Li X, Liu LF, Ku ZL, Liu TF, Rong YG, Xu M, Hu M, Chen JZ, Yang Y, Gratzel M, Han HW (2014) A hole-conductor-free, fully printable mesoscopic perovskite solar cell with high stability. Science 345:295–298
4. Wang YF, Li SB, Zhang P, Liu DT, Gu XL, Sarvarib H, Ye ZB, Wu J, Wang ZM, Chen Z (2016) Solvent annealing of PbI2 for high-quality crystallization of perovskite films for solar cells with efficiency exceeding 18%. Nanoscale. doi: 10.1039/C6NR07076K
5. Yang WS, Noh JH, Jeon NJ, Kim YC, Ryu S, Seo J, Seok SI (2015) High performance photovoltaic perovskite layers fabricated through intramolecular exchange. Science 348:1234–1237
6. National Renewable Energy Laboratory Best Research-Cell Efficiencies. http://www.nrel.gov/ncpv/images/efficiency_chart.jpg. Accessed 17 May 2016.
7. Yang Y, Song J, Zhao YL, Zhu L, Gu XQ, Gu YQ, Che M, Qiang YH (2016) Ammonium-iodide-salt additives induced photovoltaic performance enhancement in one-step solution process for perovskite solar cells. J Alloy Compd 684:84–90
8. Heo JH, Im SH, Noh JH, Mandal TN, Lim CS, Chang JA, Lee YH, Kim HJ, Sarkar A, Nazeeruddin MK, Gratzel M, Seok SI (2013) Efficient inorganic-organic hybrid heterojunction solar cells containing perovskite compound and polymeric hole conductors. Nat Photonics 7:487–492

9. Son DY, Bae KH, Kim HS, Park NG (2015) Effects of seed layer on growth of ZnO nanorod and performance of perovskite solar cell. J Phys Chem C 119: 10321–10328
10. Kang SH, Choi SH, Kang MS, Kim JY, Kim HS (2008) Nanorod-based dye sensitized solar cells with improved charge collection efficiency. Adv Mater 20:54–58
11. Zhang Y, Liu WQ, Tan FR, Gu YZ (2015) The essential role of the poly(3-hexylthiophene) hole transport layer in perovskite solar cells. J Power Sources 74:1224–1230
12. Qiu J, Qiu Y, Yan K, Zhong M, Mu C, Yan H, Yang S (2013) All-solid-state hybrid solar cells based on a new organometal halide perovskite sensitizer and one-dimensional TiO_2 nanowire arrays. Nanoscale 5:3245–3248
13. Ma TL, Akiyama M, Abe E, Imai I (2005) High-efficiency dye-sensitized solar cell based on a nitrogen-doped nanostructured titania electrode. Nano Lett 12:2543–2547
14. Li YM, Guo Y, Li YH, Zhou XF (2016) Fabrication of Cd-doped TiO_2 nanorod arrays and photovoltaic property in perovskite solar cell. Electrochim Acta 200:29–36
15. Song J, Li SP, Zhao YL, Yuan J, Zhu Y, Fang Y, Zhu L, Gu XQ, Qiang YH (2017) Performance enhancement of perovskite solar cells by doping TiO_2 blocking layer with group VB elements. J Alloy Compd 694:1232–1238
16. Zhang XQ, Wu YP, Huang Y, Zhou ZH, Shen S (2016) Reduction of oxygen vacancy and enhanced efficiency of perovskite solar cell by doping fluorine into TiO_2. J Alloys Compd 671:191–196
17. Shiva S, Raheleh M, Azam I, Nima T (2015) A new strategy on utilizing nitrogen doped TiO_2 in nanostructured solar cells: embedded multifunctional N-TiO_2 scattering particles in mesoporous photoanode. Mater Res Bull 72:64–69
18. Xie Y, Huang N, Liu Y, Sun W, Mehnane HF, You S, Wang L, Liu W, Guo S, Zhao XZ (2013) Photoelectrodes modification by N doping for dye-sensitized solar cells. Electrochim Acta 93:202–206
19. Li JF, Zhang ZL, Gao HP, Zhang Y, Mao YL (2015) Effect of solvents on the growth of TiO_2 nanorods and their perovskite solar cells. J Mater Chem A 3: 19476–19482
20. Lee MM, Teuscher J, Miyasaka T, Murakami TN, Snaith HJ (2012) Efficient hybrid solar cells based on meso-superstructured organometal halide perovskites. Science 338:643–647
21. Ito S, Zakeeruddin SM, Baker RH, Liska P, Chavet R, Comte P, Nazeeruddin MK, Pechy P, Takata M, Miura H, Uchida S, Gratzel M (2006) High-efficiency organic-dye-sensitized solar cells controlled by nanocrystalline-TiO_2 electrode thickness. Adv Mater 18:1202–1205
22. Bineesh KV, Kim DK, Park DW (2010) Synthesis and characterization of zirconium-doped mesoporous nano-crystalline TiO_2. Nanoscale 2:1222–1228
23. Zhang M, Yu XL, Lu DD, Yang JJ (2013) Facile synthesis and enhanced visible light photocatalytic activity of N and Zr co-doped TiO_2 nanostructures from nanotubular titanic acid precursors. Nanoscale Res Lett 8:543–550
24. Liu XY, Zheng HW, Zhang ZL, Liu XS, Wan RQ, Zhang WF (2011) Effect of energy level matching on the enhancement of photovoltaic response about oxide/Zn_2SnO_4 composites. J Mater Chem 21:4108–4116
25. Yao XJ, Wang XD, Su L, Yan H, Yao M (2011) Band structure and photocatalytic properties of N/Zr co-doped anatase TiO_2 from first-principles study. J Mol Catal A 351:11–16
26. Li YL, Sun WH, Yan WB, Ye SY, Peng HT, Liu ZW, Bian ZQ, Huang CH (2015) High-performance planar solar cells based on $CH_3NH_3PbI_{3-x}Cl_x$ perovskites with determined chlorine mole fraction. Adv Funct Mater 25:4867–4873
27. Archana PS, Gupta A, Yusoff MM, Jose R (2014) Charge transport in zirconium doped anatase nanowires dye-sensitized solar cells: trade-off between lattice strain and photovoltaic parameters. Appl Phys Lett 105: 53901
28. Shi Y, Wang K, Du Y, Zhang H, Gu J, Zhu C, Wang L, Guo W, Hagfeldt A, Wang N, Ma T (2013) Solid-state synthesis of ZnO nanostructures for quasi-solid dye-sensitized solar cells with high efficiencies up to 6.46%. Adv Mater 25:4413–4419
29. Wang HH, Chen Q, Zhou H, Song L, Luo S, Louis ZS, Marco ND, Fang Y, Sun P, Song TB, Chen H, Yang Y (2015) Improving the TiO_2 electron transport layer in perovskite solar cells using acetylacetonate-based additives. J Mater Chem A 3:9108–9115
30. Zhong D, Cai B, Wang XL, Yang Z, Xing YD, Miao S, Zhang WH, Li C (2015) A highly efficient zinc catalyst for selective electroreduction of carbon dioxide in aqueous NaCl solution. Nano Energy 11:409–418
31. Wang MJ, Li SB, Zhang P, Wang YF, Li HQ, Chen Z (2015) A modified sequential method used to prepare high quality perovskite on ZnO nanorods. Chem Phys Lett 639:283–288
32. Li HQ, Li SB, Wang YF, Sarvari H, Zhang P, Wang MJ, Chen ZD (2016) A modified sequential deposition method for fabrication of perovskite solar cells. Solar Energy 126:243–251
33. Liu DY, Yang JL, Kelly TL (2014) Compact layer free perovskite solar cells with 13.5% efficiency. J Am Chem Soc 136:17116–17122
34. Kim HS, Lee JW, Yantara N, Boix PP, Kulkarni SA, Mhaisalkar S, Gratzel M, Park NG (2013) High efficiency solid-state sensitized solar cell-based on submicrometer rutile TiO_2 nanorod and $CH_3NH_3PbI_3$ perovskite sensitizer. Nano Lett 13:2412–2417
35. Shogh S, Mohammadpour R, Iraji zad A, Taghavinia N (2015) A new strategy on utilizing nitrogen doped TiO_2 in nanostructured solar cells: embedded multifunctional N-TiO_2 scattering particles in mesoporous photoanode. Mater Res Bull 72:64–69
36. Chen YY, Zhang B, Feng YQ (2016) N-doped TiO_2 applied in low-temperature-based dye-sensitized solar cells. Res Chem Intermed 42: 6705–6718
37. Guo W, Shen YH, Wu LQ, Gao YR, Ma TL (2011) Effect of N dopant amount on the performance of dye-sensitized solar cells based on N-doped TiO_2 electrodes. J Phys Chem C 115:21494–21499